NUMERICAL SIMULATIONS OF AN XFELO FOR THE EUROPEAN XFEL DRIVEN BY A SPENT BEAM

J. Zemella*, J. Rossbach, University of Hamburg, Germany
C. P. Maag, DESY and University of Hamburg, Germany
H. Sinn European XFEL GmbH, Hamburg, Germany, M. Tolkiehn, DESY, Hamburg, Germany

Abstract

The European XFEL will be an X-ray free electron laser laboratory at DESY in Hamburg Germany. In the baseline design the light pulses will be generated in long undulators via the SASE process. The wavelengths of the light pulses will be between 5 nm and 0.05 nm. Since SASE pulses have a poor longitudinal coherence a lot of research is ongoing to overcome the statistical fluctuations of the SASE pulses. Some years ago Kim et al. proposed an FEL oscillator for light sources based on energy-recovery linacs (ERL), using Diamond Bragg crystals to build up a high reflective cavity in the X-ray regime (XFELO). Since the European XFEL will be based on superconducting accelerator structures it will deliver a long train of electron bunches which might be suitable to support an XFELO arrangement as well. In particular, the spent beam at the exit of a SASE FEL might be still qualified to drive an XFELO. Theoretical simulations of an oscillator based on Diamond crystals for the European XFEL will be presented using electron bunches of a spent beam.

INTRODUCTION

The beam parameters of the European XFEL allow to operate high-gain free electron lasers (FEL) [1]. Sufficient gain levels for multi pass approaches with significantly shorter undulators can be reached. For an XFELO for the European XFEL the undulator length is assumed to be less than 15 m instead of the SASE undulators which need to be at least 60 m for wavelengths of 1.5 Å and even longer for two-stage approaches [2, 3, 4]. The bandwidth of the radiation of a self-seeded XFEL or XFELO is more narrow than for SASE-FELs ($\Delta\nu/\nu \sim 10^{-3}$) and will be in the order of $\Delta\nu/\nu \approx 10^{-5} - 10^{-7}$. The pulses will have a significantly larger longitudinal coherence up to full longitudinal coherence along the photon pulse.

A cavity scheme to feed back X-ray pulses to the entrance of the undulator has been proposed for ERLs some years ago [7]. The cavity is based on Bragg deflecting crystals. Some studies have been done on cavities using Diamond crystals due to their high reflectivity and heat conduction and low thermal expansion [8, 9, 10, 11].

A numerical simulation is presented using a spent beam after a SASE undulator to generate an X-ray pulse using an XFELO. The spent beam has a significantly larger energy spread due to the emitted radiation in the SASE undulator which reduces the FEL gain [12]. The induced energy spread is approximately 10 MeV [1]. Since multi pass approaches offer a longer effective undulator length than a single pass approach it is possible to get into saturation during one pulse train containing 2600 bunches. For numerical simulation the FEL-code Ginger is used. This code offers the possibility to include the reflection characteristics of Bragg deflection crystal by an extra data file [13, 14].

Secondly, the temperature evolution of Diamond crystal absorbing XFELO like pulses considering ballistic heat transport effects is presented [18]. At cryogenic temperatures Diamond offers a high heat conduction. This is necessary to have a small temperature rise when the following pulse is absorbed. Also the free mean path increases with lower temperature [19]. At the highest thermal diffusivity at about 50 K the mean free path is about hundreds of micrometers and even at 100 K it is about tens of mircometers. If the mean free path is comparable to the thickness of the crystal, ballistic heat transfer has to be taken into account. A radial simulation code calculating the thermal evolution is modified by using an effective thermal conductivity which is valid in both regimes, diffusive resp. ballistic [18].

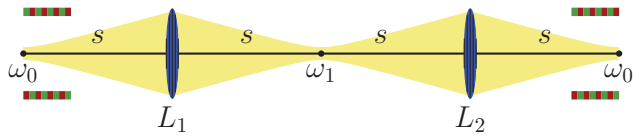

Figure 1: Schematic of one periode of the simulated unfolded crystal cavity using the Ginger FEL code. ω_0 and ω_1 referred to the waist of the photon beam in the middle of the undulator. L_1 and L_2 represents the curved Bragg deflecting crystals and s denotes the distance between the waist and the curved Bragg deflecting crystals. The green red bars refer to the undulator.

NUMERICAL SIMULATION

Ginger simulates a cavity with two curved mirrors in a certain distance (see fig. 1) and filters the radiation using the wavelengths dependent complex reflectivity of a Bragg deflection crystal, fig. 2 using the dynamical theory of X-ray diffraction from [16]. To couple out a fraction of the pulses, one crystal is thinner to transmit a part of the photon pulses. For this simulations the fraction to couple out is about 4 %. The added length to the cavity length due

* e-mail: Johann.Zemella@desy.de

ISBN 978-3-95450-123-6

Table 1: Electron Beam Parameters and Cavity Parameters Used for Numerical Simulation [15]

beam energy E_B	GeV	14.5
bunch charge q	nC	1.0
bunch length (rms) t_B	fs	75.6
peak current I_A	kA	4.9
normalized emittance ε_n	mm mrad	1.0
slice energy spread σ_E	MeV	0.45 resp. 10
energy chirp E_{Chirp}	MeV	10.0
betafunction $\beta_{x,y}$ at ω_0	m	6.0
radiation wavelength λ_R	nm	0.1029
undulator length L_U	m	15.0
undulator periode λ_U	m	0.03
cavity length L_{Cav}	m	66.62
focal length f	m	18.82
round-trip reflectivity R_{Cav}	%	87.5
output coupling T_{Cav}	%	4

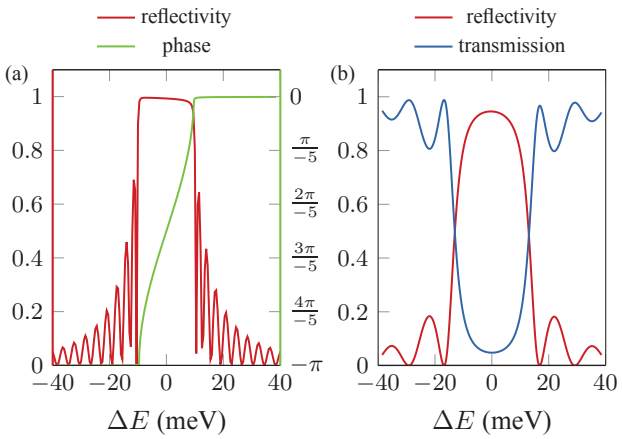

Figure 2: (a) Reflectivity of a 150 µm thick and phase of a thick Diamond crystal using the (4 4 4) reflex at 12 keV; (b) Reflectivity and transmission of a 42 µm thick Diamond crystal for the same reflection geometry using in (a).

to penetration depth of the X-rays into the crystal is artificially compensated [14]. The used electron beam and cavity parameters are listed in Tab. 1. The electron beam is symmetrically focused into the undulator in both planes (x,y) to match the photon field in the cavity. The energy chirp which is added refers from head to tail of the bunch [15].

RESULTS

Figure 3a-d shows the results of numerical simulations for an electron bunch with a charge of 1 nC whose parameters are given in Tab. 1. Both cases with a small slice energy spread $\sigma_E = 0.45$ MeV and a large slice energy spread $\sigma_E = 10$ MeV are depicted. To generate pulses with a relative small saturation energy, a small energy detuning is used since this relaxes the heat load issues. It

Table 2: Results of the Numerical Simulation for the Photon Pulses of an XFELO

rms slice energy spread σ_E	MeV	0.45	10.0
detuning parameter η	$\cdot 10^{-4}$	0	6.36
gain per passage		1.1	0.105
round-trips to saturation		26	190
photon pulse energy E_P	µJ	286	211
rms photon pulse length t_P	fs	42.8	52.2
relative spectral width f_{rel}	$\cdot 10^{-7}$	8.17	7.6
time bandwidth product		0.64	0.73
photon beam size at ω_0 σ_{ω_0}	µm	14.0	
photon beam size at L_1 σ_{L1}	µm	39.2	
opening angle θ_R	µrad	2.33	
couple out photon per pulse	$\cdot 10^9$	5.93	4.37
peak brilliance PB	B $\cdot 10^{34}$	1.1	0.69

is possible to get much larger stored energy but this will heat up the crystals too high. For the case of a small energy spread $\sigma_E = 0.45$ MeV the relatively energy deviation is $\eta = 0$; the XFELO runs at resonance energy. The photon pulse energy saturates after 26 cavity round-trips at about $E_{Phot} \approx 286$ µJ (fig. 3a). At saturation the photon pulses are almost fully coherent in the transversal direction due to its almost perfect Gaussian shape in radial direction (fig. 3b). In the longitudinal direction the photon pulses have a smooth nearly Gaussian shape in comparison to SASE pulses with their spiky structure [1]. The photon pulses have little noise at the maximum. The rms pulse length of the photon pulse is $t_P = 42.8$ fs (fig. 3c). In comparison with the length of the electron bunch the photon pulse length is about 60 %. One trailing pulse with lower amplitude can be observed. This pulse is generated through multiple reflections at the crystal surfaces [14]. The rms relative spectral width of the pulses is $f_{rel} = 8.17 \cdot 10^{-7}$ rms (fig. 3d). At the edges of the pulses the Gaussian shape is distorted. The distortion at the right edge is larger due to slightly asymmetric reflection of the crystal. The simulation shows a time bandwidth product of about 0.64 assuming a lower limit of 0.5. The peak brilliance is about $PB \approx 1.1 \cdot 10^{34}$ B (B = $\frac{\text{photons/s}}{\text{mm mrad } 0.1\% \text{ BW}}$).

Increasing the slice energy spread to $\sigma_E = 10.0$ MeV the gain is reduced by a factor of 10 for a detuning of $\eta = 6.36 \cdot 10^{-4}$. This leads to a saturation energy of $E_{Phot} \approx 211$ µJ after 190 cavity round-trips. The transversal pulse profile is also nearly Gaussian with a slight flat top at the maximum which indicates high transversal coherence. The temporal profile has almost the same shape with lower amplitude comparing with the low energy spread case. The pulse duration is slightly larger with $t_P = 52.2$ fs (fig. 3c). The spectrum of the pulses has the same distortions at the edges of the pulses. The relative spectral width of the pulses is slightly smaller $f_{rel} = 7.6 \cdot 10^{-7}$ due to its longer temporal profile. The time bandwidth product is about 0.73. The pulses have a peak brilliance of $PB \approx 0.69 \cdot 10^{34}$ B.

ISBN 978-3-95450-123-6

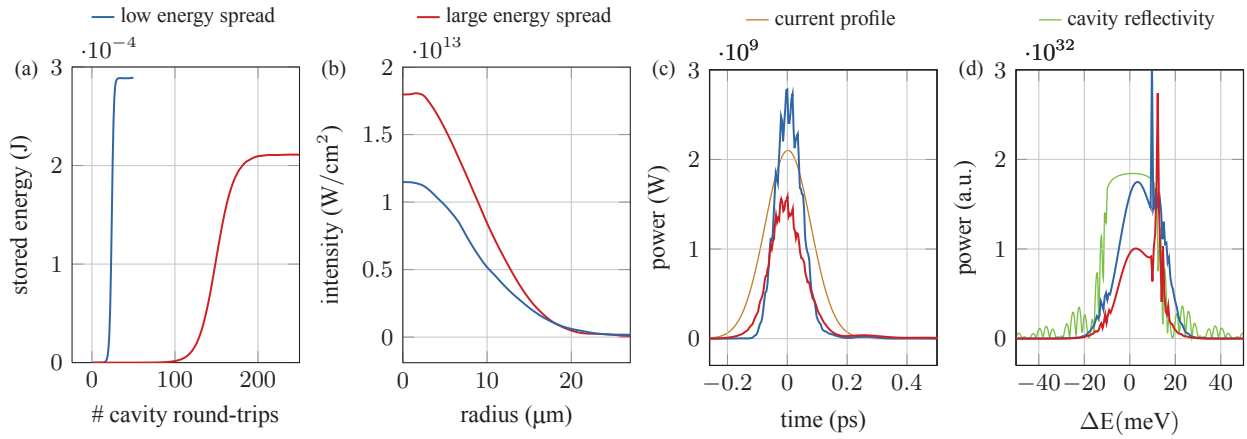

Figure 3: The results of numerical simulation with an electron bunch with a charge of 1 nC (see Tab. 1); (a) Stored photon pulse energy versus number of cavity round-trips; (b) Intensity of photon pulse at saturation versus radial position of simulated grid at the center of the undulator; (c) Power of photon pulse at saturation in time domain at the end of the undulator; (d) Power of photon pulse at saturation in frequency domain at the end of the undulator. The large energy spread case describes the case of a spent beam from a SASE FEL (red).

THERMAL BEHAVIOUR OF THE DIAMOND CRYSTAL

The temperature evolution of the crystal is calculated by the Fourier law for diffusive heat transport $q = -\lambda \nabla T$ with heat flux q, thermal conductivity λ and temperature gradient ∇T [17]. Considering ballistic heat transport an effective thermal conductivity is introduced [18]

$$\lambda_{\text{eff}}(T) = \frac{\lambda(T)}{\frac{4}{3}\frac{l(T)}{L} + 1}$$

with crystal thickness L, mean free path $l(T) = 3\lambda(T)/c_{\text{v}}(T)v_{\text{s}}$, thermal conductivity $\lambda(T)$ [19], specific heat per unit volume $c_{\text{v}}(T)$ and speed of sound v_{s} [17]. In the ballistic regime the phonons scatter only at the boundaries of the bulk which is assumed to be black in sense of photon radiation [18].

The radial grid size of the simulation is 1 cm using a grid spacing of 4 μm. The thickness of the bulk in the center region is $L_{\text{C}} = 42\,\mu\text{m}$ which corresponds to the thickness of the thin Diamond crystal to couple out radiation and a thickness of $L_{\text{C}} = 150\,\mu\text{m}$ accordingly to the thicker crystal. At a radius of 2.5 mm the thickness increases to $L_{\text{Edge}} = 5\,\text{mm}$. The absorbed energy is assumed to be uniform in depth. This assumption reduces the maximal temperature rise after absorbing the pulse energy. The absorbed pulse energy is set to $E_{\text{Abs}} = 2.0\,\mu\text{J}$ which corresponds to $\sim 1\,\%$ of absorption of the crystal assuming the saturation energy from slice energy spread Tab. 2. Effects due to high temperature gradients are neglected which reduces the likely thermal conductivity.

Figure 4a shows the results for a thickness of $L_{\text{C}} = 42\,\mu\text{m}$, pulse separation of $t_{\text{sep}} = 222\,\text{ns}$ and spot size of $\sigma_{\text{r}} = 39\,\mu\text{m}$ for the temperature at the center just before the next pulse encounters the surface for two different crystal temperatures. After 100 microseconds the temperature of a Diamond including ballistic heat transport for an initial temperature of $T_0 = 50\,\text{K}$ is about $T = 72.6\,\text{K}$ and for an initial temperature of $T_0 = 100\,\text{K}$ is about $T = 115.5\,\text{K}$. The diffusive heat transport equation leads to temperatures $T = 53.6\,\text{K}$ for $T_0 = 50\,\text{K}$ and $T = 110.8\,\text{K}$ for $T_0 = 100\,\text{K}$.

Figure 4b shows the same for a 150 μm thick crystal. Due to the thicker crystal the temperature rise becomes smaller since the absorbed energy density is lower. Even for a thicker crystal and lower thermal gradients the ballistic heat transport has an impact on the temperature evolution. The ballistic diffusive heat transport resp. diffusive lead to a temperature of $T = 103.7\,\text{K}$ resp. $T = 103.3\,\text{K}$ for an initial temperature of $T_0 = 100\,\text{K}$ and $T = 53.6\,\text{K}$ resp. $T = 51.4\,\text{K}$ for an initial temperature of $T_0 = 50\,\text{K}$.

Figure 5a-b shows the temperature of the crystal just before the following pulse is absorbed for an increased pulse separation time of 444 ns and 666 ns for the thin and thick crystal. Even for such long separation times and a thicker crystal, ballistic heat transport has a visible contribution and leads to slightly larger crystal temperatures.

CONCLUSION

The numerical simulation of an XFELO at 1 Å, using the 2D FEL code Ginger, shows that it would be possible to drive an XFELO using a spent beam, which already generated a SASE pulse in a SASE undulator in front of an XFELO. The saturation energy could be adjusted using the relative energy deviation η to achieve a relatively small saturation energy. The gain decreases by a factor of 10 for an electron bunch with a large energy spread compared to the gain of the small energy spread electron bunch. The bandwidth of the pulses generated with an 75 fs long elec-

ISBN 978-3-95450-123-6

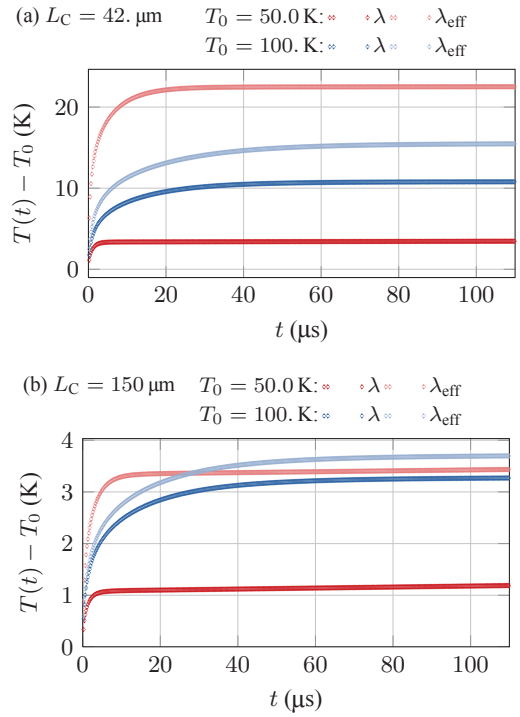

Figure 4: Temperature of a Diamond crystal before absorbing the following 2 µJ pulse with an rms width of 39 µm and pulse seperation of 222 ns for a crystal thicknes of (a) 42 µm and (b) 150 µm.

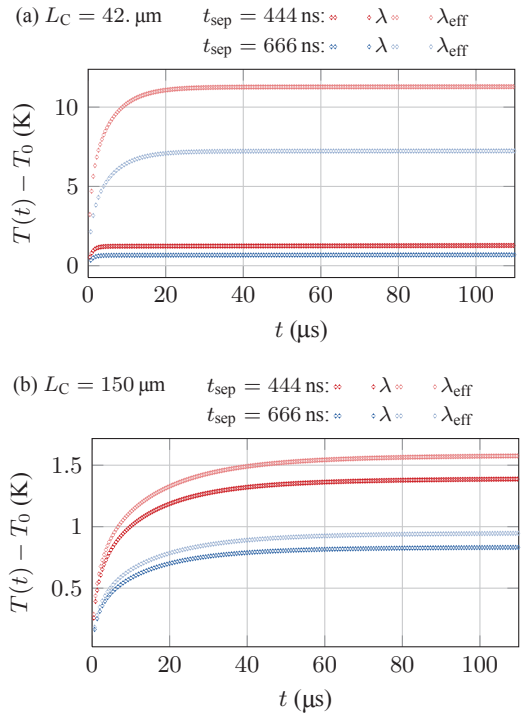

Figure 5: Temperature of a Diamond crystal before absorbing the following pulse for different pulse separation times of (a) 42 µm and (b) 150 µm thickness.

tron bunch is 8 meV rms. The pulse is nearly Fourier bandwidth limited. The peak power at saturation is in the order of $1 - 3$ GW. There is noticeable noise at the maximum of the temporal profile. Also there are some spiky distortions at the edges in the spectrum which have a larger spectral density than the broad spectrum.

The heat load simulations considering ballistic heat transport show differences to diffusive heat transport. For this calculation the spontaneous undulator radiation is not included which increases the temperature. In case of a thin Diamond crystal and a pulse separation time of 222 ns a temperature rise of more than 20 K have to be expected. In this temperature range the thermal expansion is in the order of $10^{-8}\,K^{-1}$. This temperature rise would lead to a shift of the Bragg energy of about $\Delta E/E \approx 3 \cdot 10^{-7}$. This relative energy change might be acceptable. For 100 K the energy change is more than ten time higher which is larger than the Darwin width of the used Diamond crystal. For longer pulse separation times and thicker crystals the temperature change is smaller and therefore the Bragg energy change will be smaller. One has to mention that the diffusive ballistic heat transport may still overestimates the heat flux observed experimentally as shown in the case of thin silicon layers in [20].

REFERENCES

[1] M. Altarelli et al., DESY Report 2006-097 (2007).
[2] D. Ratner et al., Proc. of FEL 2009, TUOA03, UK.
[3] G. Geloni et al., DESY Report, 10-239 (2010).
[4] J. Amann et al., Nat Photon. ad. online publ. (2012).
[5] E. L. Saldin et al., Nucl. Inst. and Meth. A **475** (2001) 357.
[6] G. Geloni et al., DESY Report 10-053 (2010).
[7] K. J. Kim et al., PRL **100** (2008), 244802.
[8] Y. Shvyd'ko et al., Nat. Phys. **6** (2010), 196.
[9] L. Wei, P. et al., PRL **70** (1993), 24.
[10] G. A. Slack et al., J. Appl. Phys. **46** (1975) 89.
[11] S. Stoupin et al., PRL **104** (2010) 085901.
[12] M. Xie, Nucl. Inst. and Meth. A **445** (2000) 59.
[13] W. M. Fawley, Lawrence Berkeley Laboratory Technical Report No. LBNL-49625.
[14] R. R. Lindberg et al., Phys. Rev. ST A&B **14** (2011), 010701.
[15] I. Zagorotnov, "Beam Dynamics and SASE Simulations for XFEL", Talk at beam dynamics meeting, DESY (2011).
[16] Y. Shvyd'ko, "X-Ray Optics High-Energy-Resolution Applications", Springer-Verlag (2004).
[17] C. Kittel. "Introduction to Solid State Physics". J. Whiley & Sons (1986).
[18] A. Majumdar. J. Heat Trans. **115** (1993) 7.
[19] V. B Efimov et al. Physica B **263** (1999) 745.
[20] M. Ashegi et al., J. Heat Trans. **120** (1998) 30.

ISBN 978-3-95450-123-6